Hindawi
Modelling and Simulation in Engineering
Volume 2024, Article ID 7142460, 19 pages
https://doi.org/10.1155/2024/7142460

Research Article

Finite Element Modelling and Simulation of Tunnel Gates of Dam Structures in ABAQUS Using Reduced-Integrated 8-Node Hexahedral Solid-Shell Element

Can Balkaya

BUPIM International Project & Consulting Co., 06450 Ankara, Türkiye

Correspondence should be addressed to Can Balkaya; can@bupim.com

Received 9 February 2024; Revised 10 March 2024; Accepted 1 April 2024; Published 6 May 2024

Academic Editor: Jean-Michel Bergheau

Tunnel gates used for water regulation are very important and critical parts of dam safety. This is because they are exposed to the hydrostatic pressure of the total height of the water in the reservoir. In this case study, a nonlinear finite element modelling and simulation of the diversion tunnel gate of the Gokdere Bridge Dam in Adana, Turkey, are performed to investigate the performance and capacity of the structure before collapse. The maximum water level in the reservoir is 85 meters. A 3D finite element modelling of the gate structure was created, considering the details of the construction project. Both the concrete structure and the anchorages between the concrete of the first and second phases of the gate structure and the steel profiles in the gate supports are modelled to obtain composite behavior, bond stresses, and a more accurate load and stress distribution. For the nonlinear finite element modelling in ABAQUS, C3D8R reduced-integrated 8-node hexahedral solid elements with concrete damage and tension stiffening are used. For the simulation, linear and nonlinear capacity analyses of the gate structure are performed, and the stresses, strains, deformations, and crack propagation in concrete and steel are investigated. It is found that nonlinear analysis and finite element modelling of anchors for capacity and load transfer are important in the simulation of gate structures to prevent tunnel collapse. It is suggested that dam monitoring and control systems and the use of multiple gates are recommended when a problem occurs in the operation of a gate in the diversion tunnel gates of a dam structure.

1. Introduction

The safety of dams depends largely on the safety of their gates. The number of dams with gates for the efficient use of water is increasing. More than a third of all large dams have gates, and most of these are flood control dams that regulate floods and other water discharges. The invention and earlier use of gates date to 1490 [1]. The most common types of vertical lift gates used for hydraulic structures are stone gates, tracked gates, gates with fixed wheels, and sliding gates. Vertical lift gates with wheels on the sides to reduce friction are called fixed wheel gates, while gates without wheels are called sliding gates. A radial gate differs from a flat gate, an arm gate, which is used in both dams and canal locks to control the flow of water. A method for developing an optimal design of radial gates using steel sections and different types of steel was investigated [2].

The gates are mainly used for operational, emergency, and maintenance purposes in dams or irrigation canals. An optimal design of the lifting mechanism and a well-equipped and efficient control system for lifting the gate are also important. The two-dimensional dam failure analysis of Berdan Dam for floodplains and the preparation of emergency plans using GIS data are presented by Unal [3]. It is also important to control the water in the tunnel gates of dams in case of flooding. If the gate fails or does not open at the required speed, this poses a major problem for the dam [4] and ultimately for public safety.

The standards and regulations for dam construction do not address the connection between the gate and the main

Figure 1: Structure of the diversion tunnel and gate.

reinforced concrete structure [5–7]. Only the standards require a 3D analysis and design for the tunnel and diversion structures in Section 2.2 of reference [5]. The design analysis of water protection sliding gates for diversion dams is investigated using CFD and ANSYS [8, 9]. The novelty of this research work is that there is no published work on 3D finite element modelling and simulation of tunnel gate structures including their connections and construction phases, which are very important and critical parts of dams exposed to the maximum water level in the reservoir. A case study with real details of the construction project for nonlinear finite element modelling and simulation of the diversion tunnel gate of Gokdere Bridge Dam in Adana, Turkey, is presented.

On the other hand, there are many studies on concrete damage models, experimental and numerical solutions, and failure and seismic analysis of dams for dam safety. By combining experiments and numerical solutions, the damage characteristics of the dam body under the action of various water explosions are investigated for a 50-meter-high gravity concrete dam [10]. A damage analysis for arch concrete dams with underwater explosion loading is carried out [11]. A plastic damage model for the cyclic loading of the concrete was developed by Lee and Fenves [12] for the seismic analysis of the concrete dams. Mesoscale 3D fracture modelling and validation of the concrete based on in situ X-ray computed tomography images using a damage plasticity model [13] with damage and fracture profiles and for damage calculations [14] with Monte Carlo simulations of the dynamic compressive behavior of the concrete are investigated. In the mesomodels, the damage usually starts around the largest voids.

Figure 2: View of the diversion tunnel from the dam reservoir.

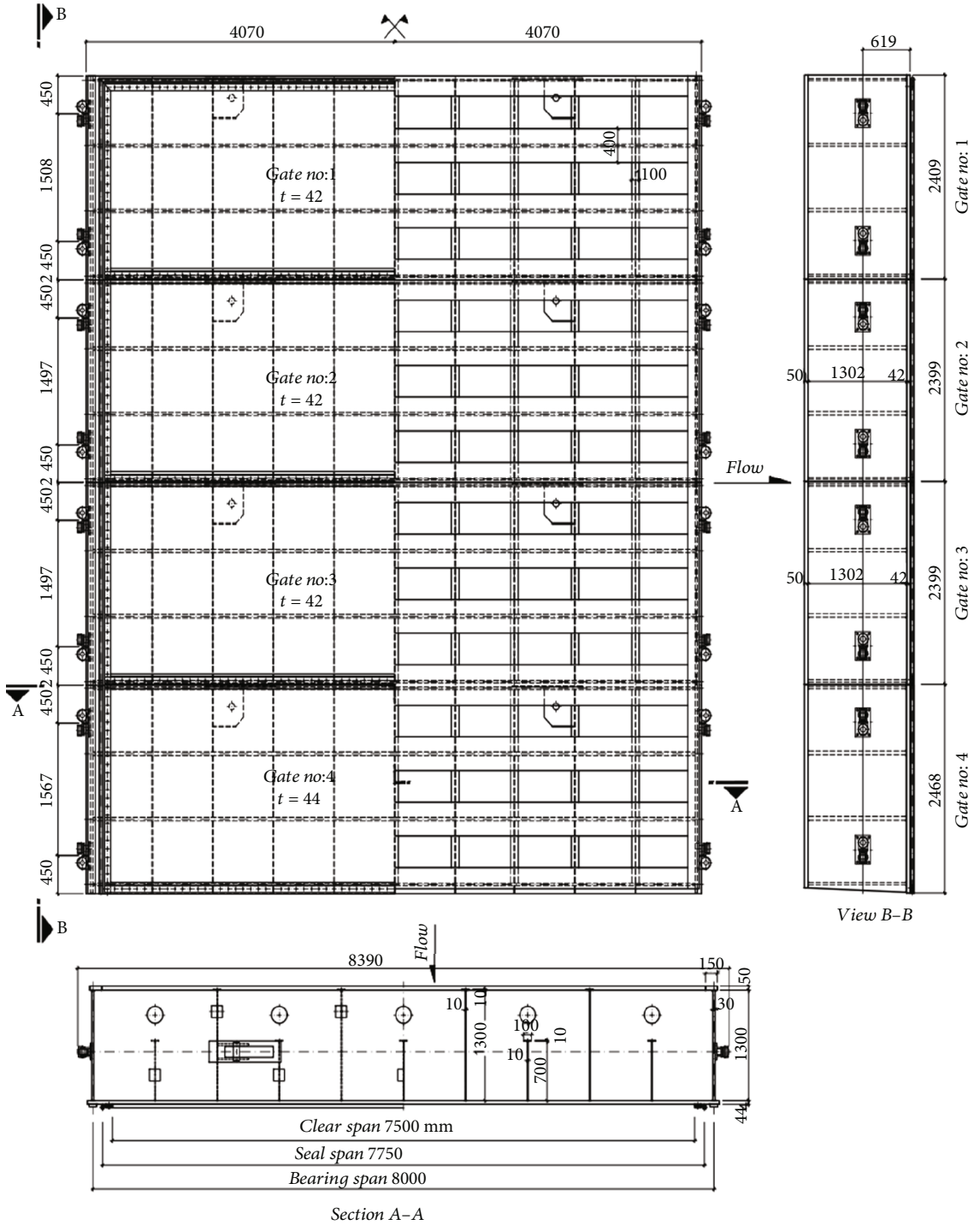

Figure 3: Detail of diversion tunnel steel stoplog gates (four leaves) with guide roller.

2. Case Study: Structural Information about the Diversion Tunnel and the Gate of the Gokdere Bridge Dam, Adana, Turkey

In this case study, the 3-dimensional ABAQUS [15] finite element structure of the diversion tunnel gate of the Gokdere Bridge Dam Project in Adana was analyzed with a computer program for structural analysis and linear and nonlinear capacity analysis at a water level of 85 meters in the reservoir. The ABAQUS finite element model was developed based on the structural details of the diversion tunnel gate shown in Figure 1. A view of the diversion tunnel from the bridge dam reservoir is shown in Figure 2. As you can see, the gates are subjected to the hydrostatic pressure of the total height of the water in the reservoir. Their behavior and design are important for the safety of the dam. The steel

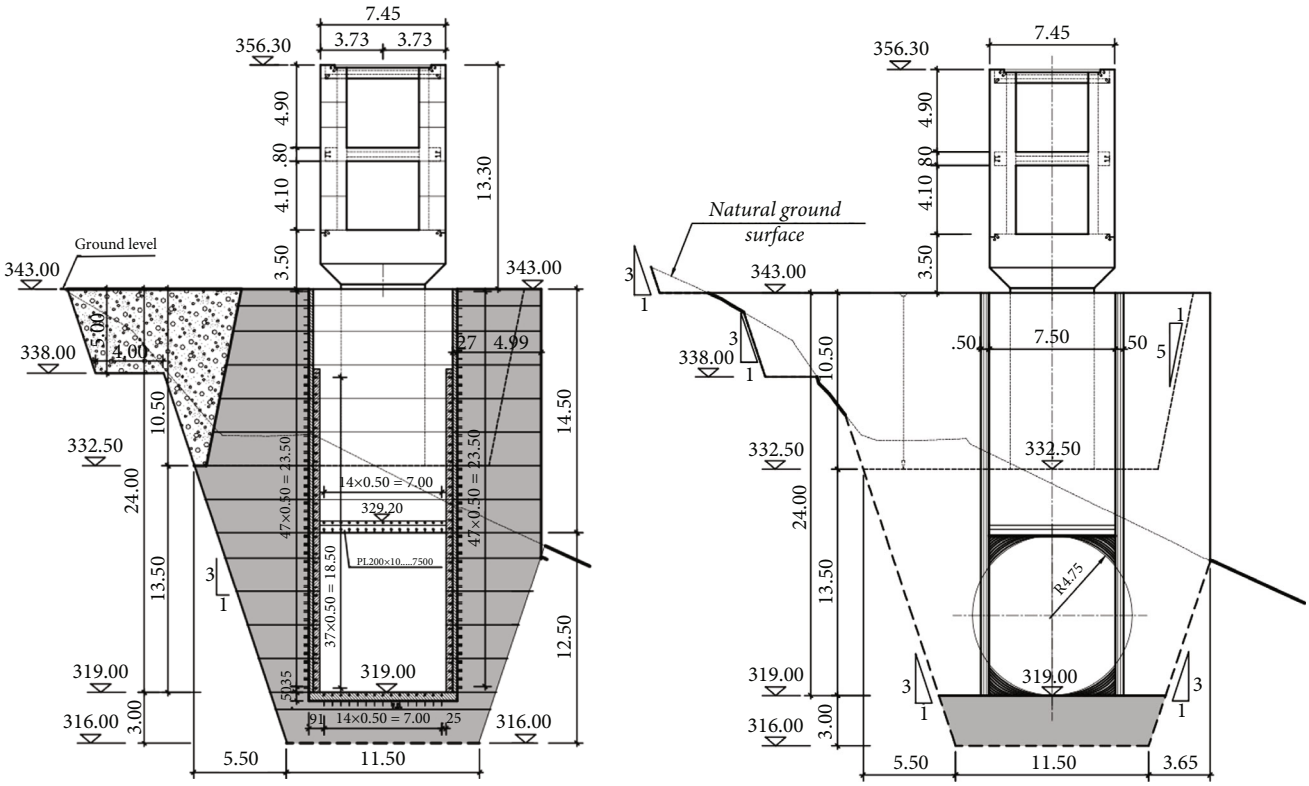

Figure 4: The sections and front view of diversion tunnel gate structure.

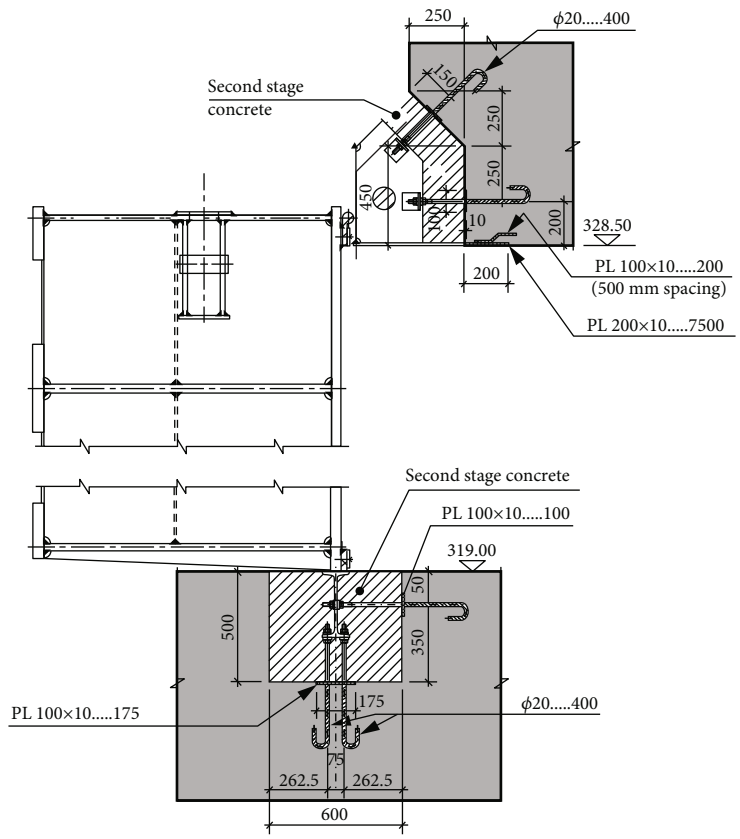

Figure 5: Detail 1: steel plates and anchor connections in the first and second phases of the concrete.

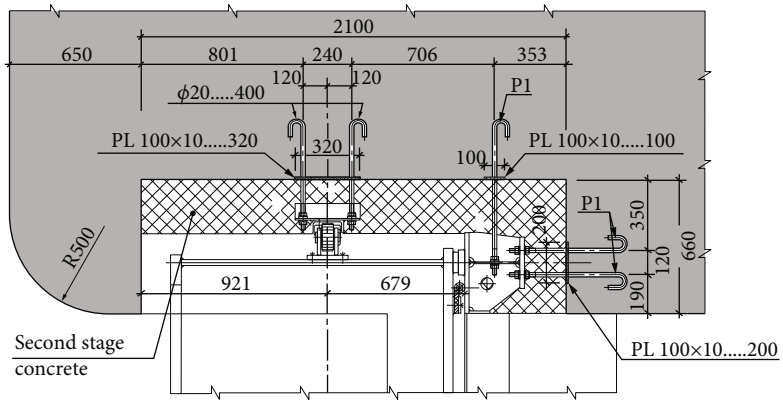

Figure 6: Detail 2: steel plate and anchor connection in the first and second phases of the concrete.

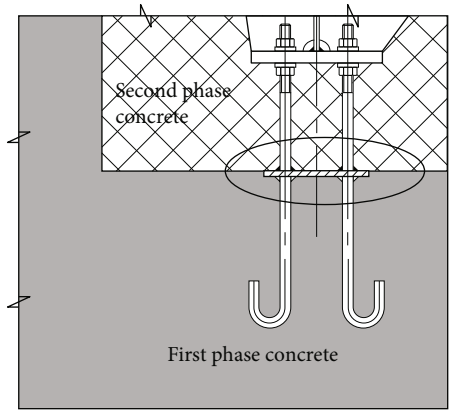

Figure 7: Plate and anchor connection in the first and second phases of the concrete.

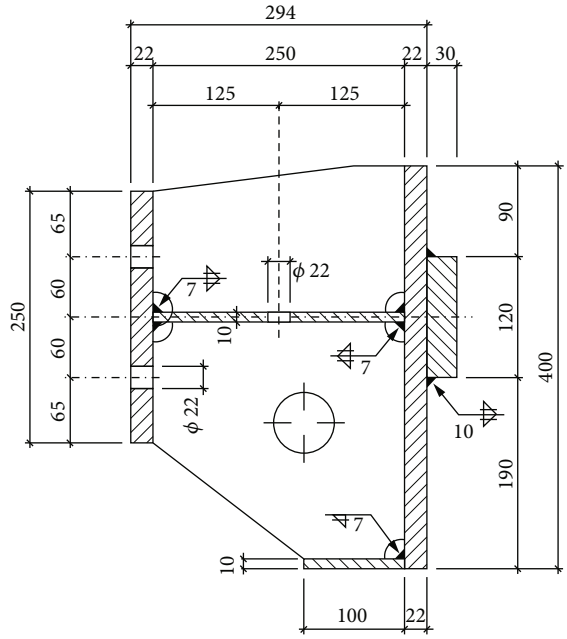

Figure 8: Dimensions of the I-profile on the gate and welding condition of the steel connection.

gates (four wings) of the diversion tunnel are sliding gates with guide rollers (see Figure 3). Rubber seals on the four downstream sides ensure water tightness. The gates are moved by a mobile crane. The first gate, the second gate, and the other gate wings are lowered, and the water in the diversion tunnel is stopped when the gate is closed (see Figure 1).

Below you will find the project drawings and reinforced concrete details of the gate structure of the diversion tunnel. The sections and the front part of the reinforced concrete gate structure of the diversion tunnel are shown in Figure 4 with dimensions and elevations. Figures 5–7 show the concrete of the first and second phases and the details of the steel anchor connections used in the construction. In the figures, the gray part is the first phase of the concrete structure and the shaded part is the second phase of the concrete structure.

In the construction project, the anchors and their plates remain in the first phase of the concrete (the gray part in Figure 7). Before the concrete of the second phase is placed, the remaining anchors are mounted on slabs and steel sections. In order to transfer the load of the gates to the concrete of the first and second phases and the load of the gates to the bond with the steel plates and the anchors, the welding of the buried plates should be done by the technique and the load should be transferred, the buried

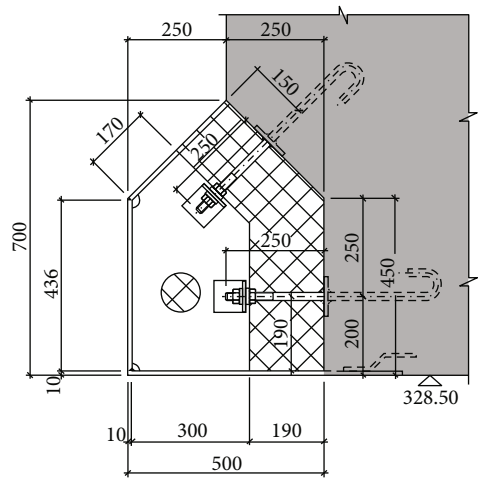

Figure 9: The thickness of the beam is 250 mm and under the beam where the gate lies.

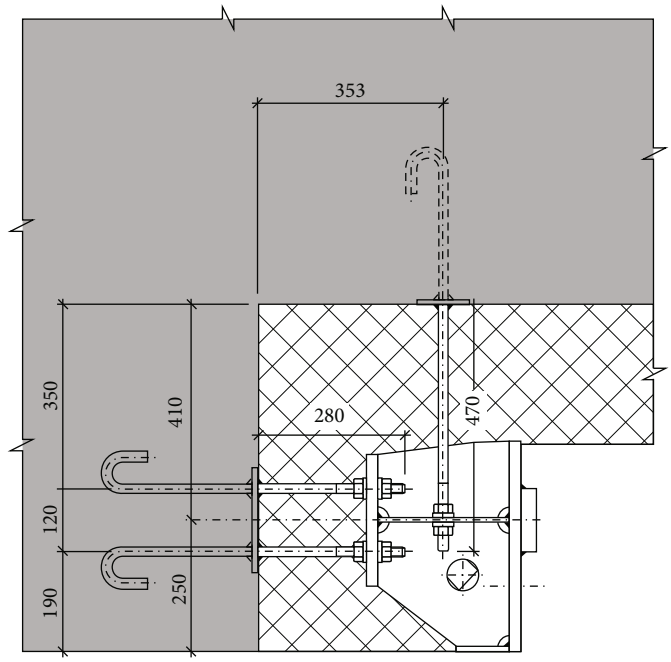

Figure 10: Anchorage lengths and types.

plates should be placed as shown in the project, and the steel profiles in which the gates are inserted should be matched to these anchors and replaced properly.

The condition of the upper and lower flanges of the steel I-profile into which the gate is pressed is as follows: upper flange: one piece, 22 mm thick, and 400 mm wide and lower flange: 22 mm thick and 250 mm wide. In addition, the head of the flake lying in the direction of flow is 100 mm. The weld seam thickness of the lower flange of the I-profile is 10 mm. The weld seam of the upper and lower flanges of the I-profile is 7 mm. These welds are circumferential (Figure 8). The anchors, which determine the behavior of the composite system with the concrete and steel elements of the 2nd phase, are important for the anchors.

There is a steel plate on the underside of the beam that ensures tightness and to which the steel plate should be attached. The thickness of the beam is 250 mm, as shown in Figure 9. The anchorage lengths and types in phase 1 and phase 2 of the concrete are shown in Figure 10.

3. Linear and Nonlinear Finite Element Modelling of Tunnel Gates of Dam Structure

A model containing all elements (steel plate and section, anchors, and concrete) and nonlinear elastic properties of the materials is created to see the real behavior of the composite structure for the 3D finite element model of the gate structure. The concrete thicknesses, number of anchors and dimensions, steel plate, and profile dimensions are also considered in a detailed project. Nonlinear analyses were performed to show the actual behavior and strength of the structure.

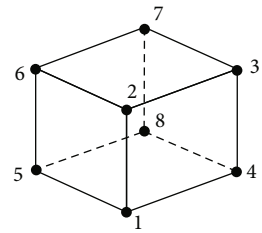

C3D8R: continuum, 3D, 8-node, reduced integration

Figure 11: ABAQUS C3D8R reduced-integrated 8-node hexahedral solid-shell element.

For the linear and nonlinear finite element modelling in ABAQUS [15], the gate structure is considered in the 3-dimensional finite element model, as shown in Figures 1 and 2, considering the details of the design project. This is important for the behavior of the composite structure. The analyses performed in the ABAQUS model were also performed using the nonlinear analysis method. The hydrostatic loads from the gate were transferred through steel plates, sections, and anchors with composite material and nonlinear behavior.

The structure of the tunnel gate consists of two-phase concrete and is supported by I-beams and anchors. This structural model is analyzed using the 3D finite element method. For this purpose, the universal finite element program ABAQUS is used for the modelling of the concrete and steel elements. The 3D C3D8R hexahedral solid elements shown in Figure 11 are used. To model the system realistically, the dimensions of the elements are set to approximately 5 cm. Each finite element has 8 nodes, an isoparametric property, and a reduced integration capacity.

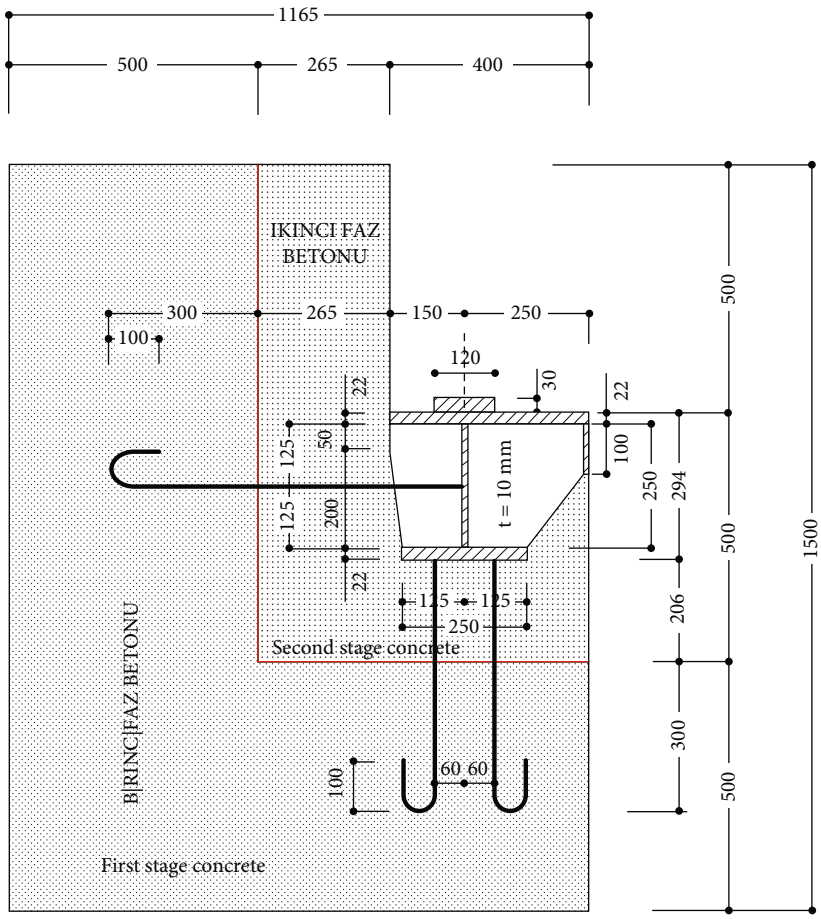

Figure 12: Dimensions of the model of the gate structure (anchoring and spacing of the plates in the vertical direction: 500 mm; height of the model in the third dimension: 2 m).

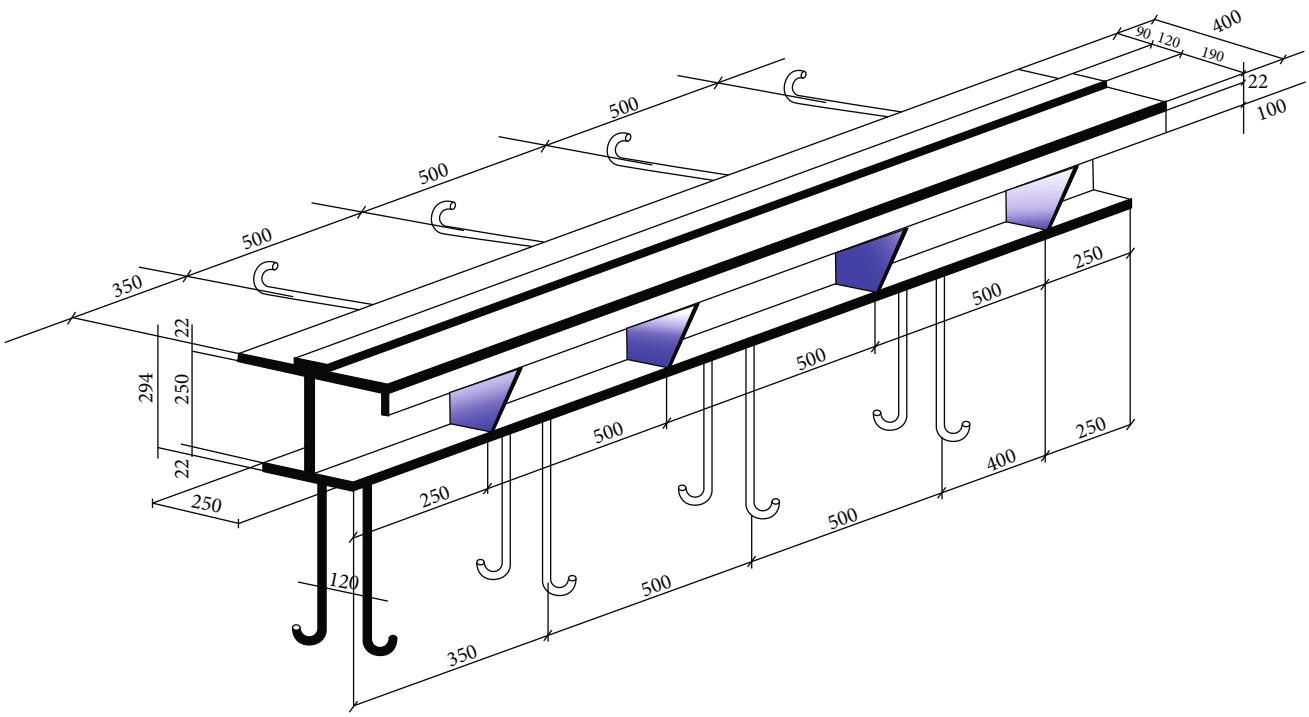

Figure 13: Steel profiles, plates, and anchoring dimensions (for a 2 m long piece).

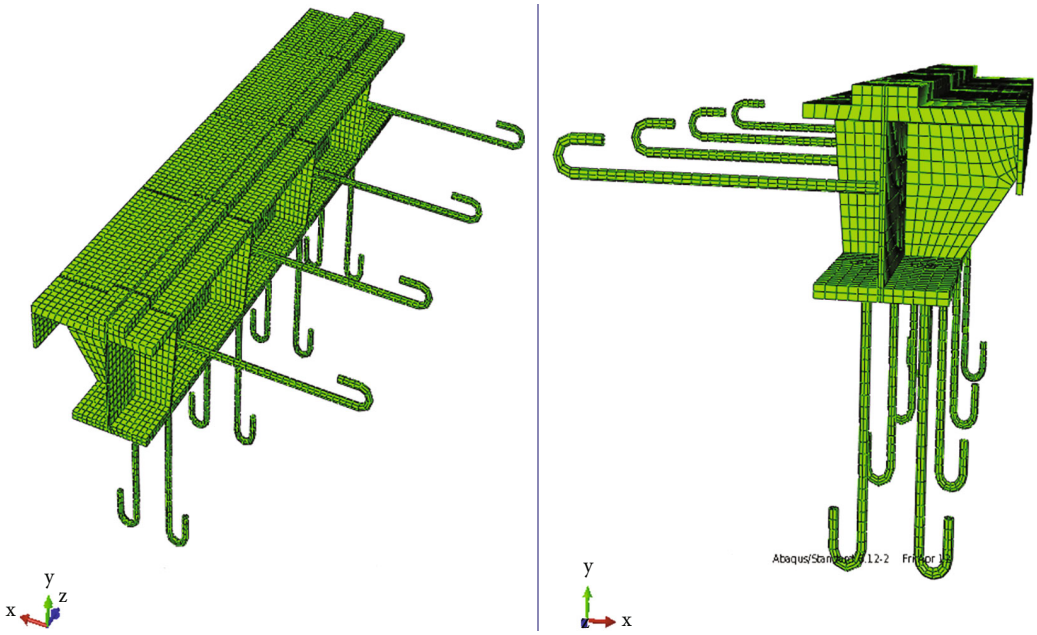

Figure 14: Steel sections, plates, and anchorage patterns.

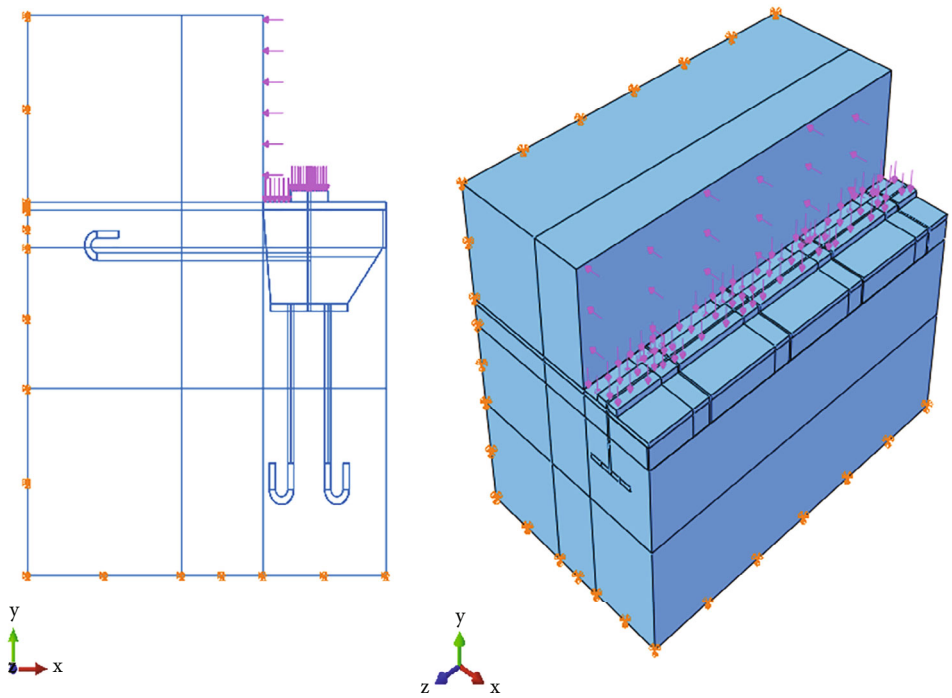

Figure 15: Load and boundary conditions in the ABAQUS model.

For the concrete damage plasticity (CDP) model in ABAQUS, the actual definition of the material model and the main parameters and the definitions of the properties are required to define this material model, simulate the elastic and plastic response, simulate damage, and simulate failure. The damage property refers to the degradation of stiffness during unloading/reloading. This property is a suboption of CDP and can be ignored when dealing with monotonic loading. The simulations of elastic property, plastic property, and damage property in ABAQUS are defined as follows: (1) elastic property or the elastic material response; (2) plastic property, defined as the stress-strain behavior in the plastic or inelastic range and basically defines other parameters; and (3) the damage property which refers to the deterioration of the material's relief stiffness under cyclic loading. If it is a monotonic loading scenario, this property definition can be ignored. The default values for the definition of plasticity properties in ABAQUS are used. To define

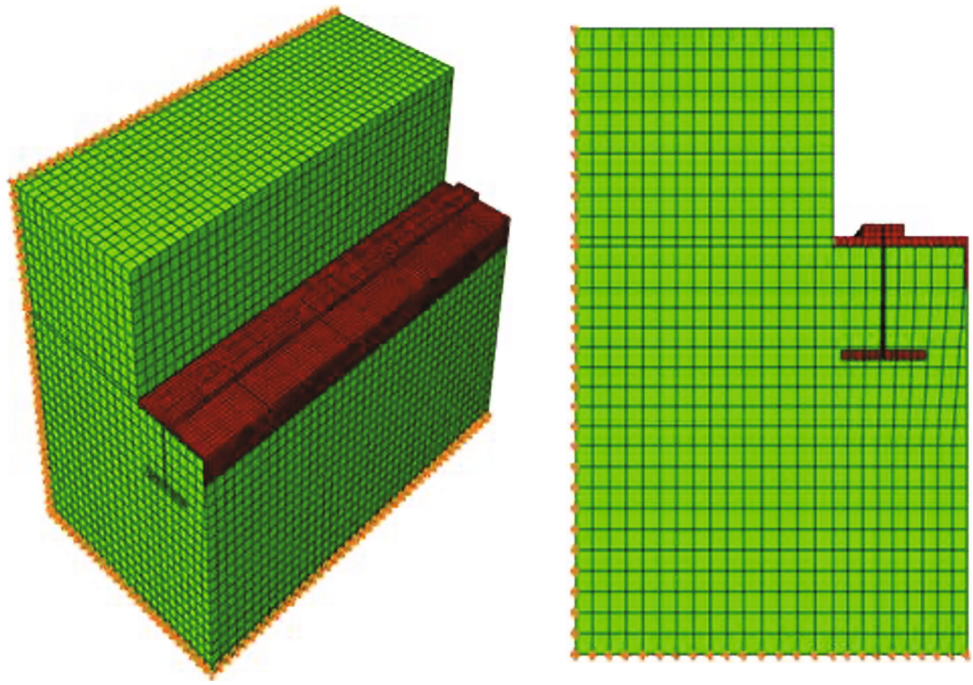

Figure 16: Boundary conditions of the finite element model.

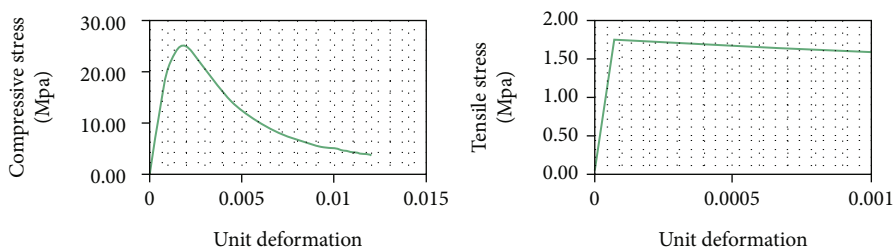

Figure 17: Material models for nonlinear analysis of the concrete.

the failure of the concrete material, add the damage definition TYPE = Strain to the input file, with the failure strain at cracking, the failure strain at compression in elastic form, and the corresponding damage values at which failure is assumed.

"CONCRETE" defines concrete properties outside the elastic range.

"CONCRETE COMPRESSION DAMAGE" defines the compression damage properties for the damaged plasticity model of the concrete.

In nonlinear analysis, the terms "Concrete damaged plasticity", "Concrete tension stiffening", "Concrete tension damage", and "Concrete compression damage" are used.

For the behavior of contact surfaces, "SURFACE INTERACTION" with the option "GAP" or "INTERFACE" is specified in the ABAQUS Keywords Reference Manual [16]: "CONTACT CONTROLS", "GAP", "INTERFACE", AND "SURFACE INTERACTION". Friction behavior for surface-based contact, when the surfaces are in contact, normally transmits both shear and normal forces across their interface with the "SURFACE INTERACTION" and "FRICTION" command. The active D.O.F. 1, 2, 3, 4, 5, and 6 were

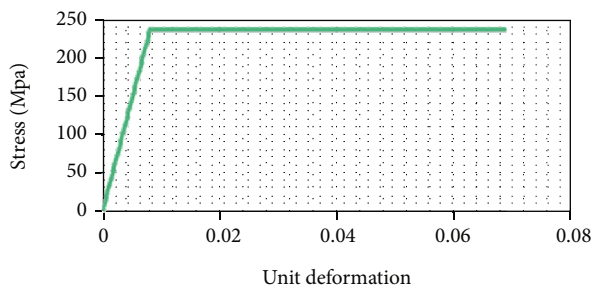

Figure 18: Elastoplastic stress-strain behavior of steel.

used for the connecting element. The steel profile is subject to the same degree of freedom at all contact points for load transfer and the bond between anchor elements and concrete.

Explicit modelling of the interface between steel and concrete is of greater importance for the interaction of composite materials. Hai et al. [17] explicitly simulate the bonding and debonding behavior at the interface for mesoscale failure mechanisms of ultrahigh strength fiber-reinforced concrete. Another approach is to explicitly model the

Table 1: Material properties used in the finite element analysis.

Materials	Elastic module (MPa)	Compressive strength (MPa)	Tensile strength (MPa)	Yield strength (MPa)	Poisson ratio
Concrete C25	23500 (Popovich model, nonlinear analysis)	25	1.75	—	0.2
	30000 (linear analysis)	—	—	—	
Steel profile St37	206180	—	—	235	0.3
Reinforcement St1	200000	—	—	220	0.3

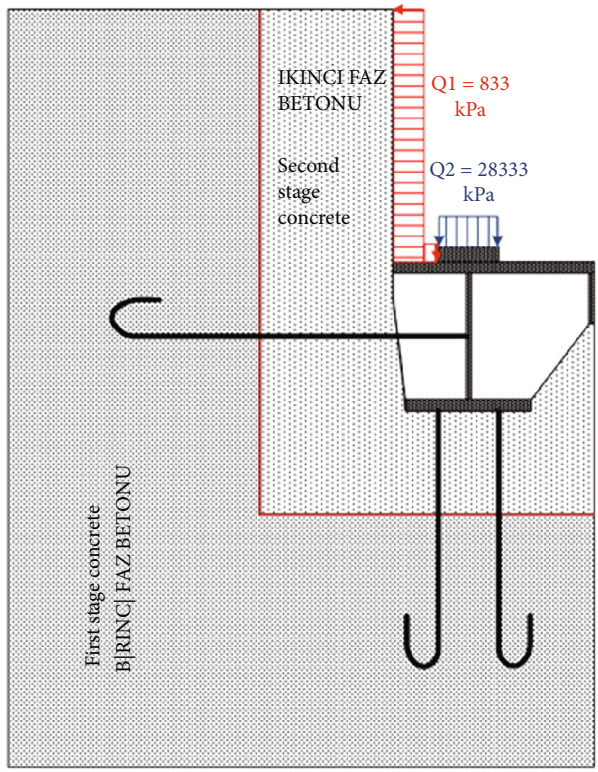

Figure 19: Applied pressure loads to the finite element model.

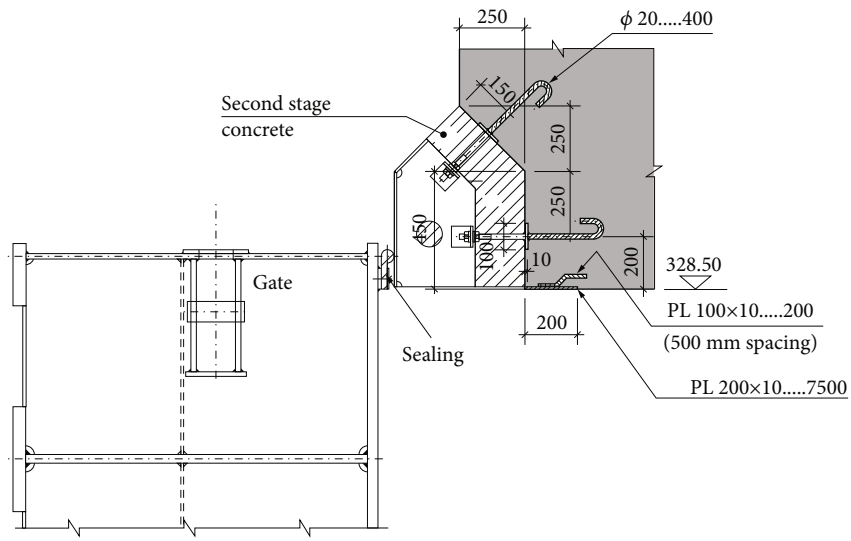

Figure 20: Detail of the sealing at the top of the gate.

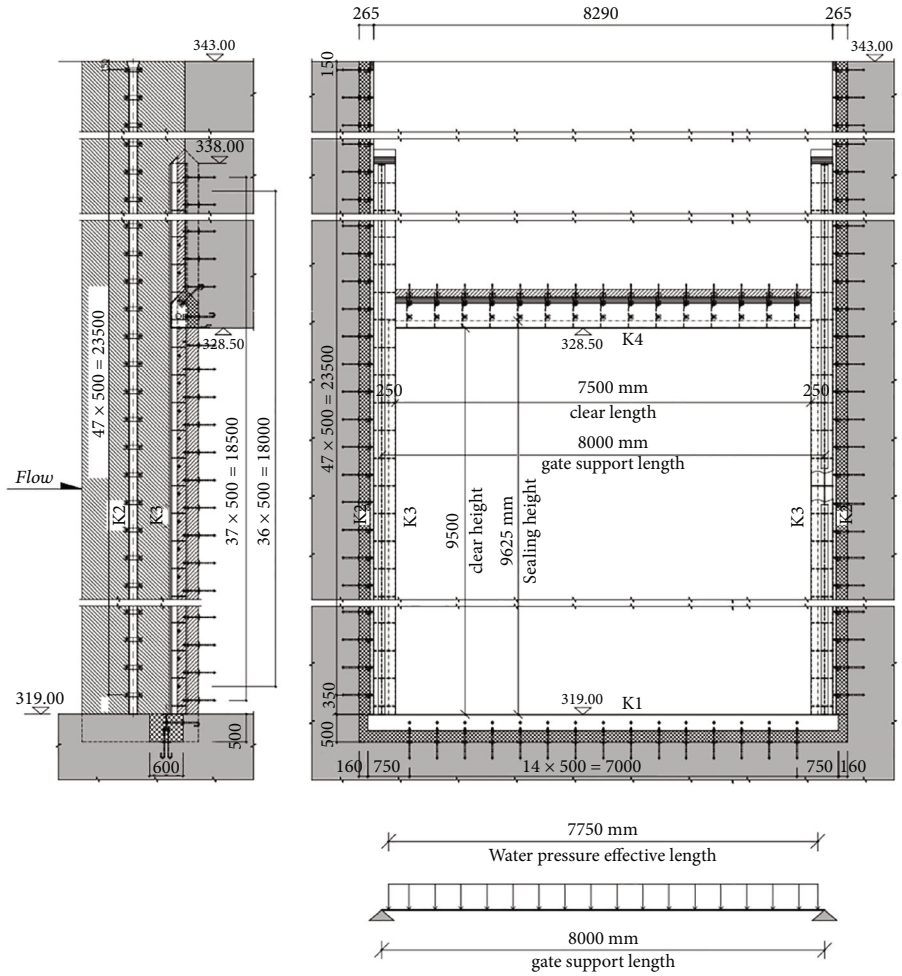

Figure 21: Lateral supports and load distribution on the gate structure.

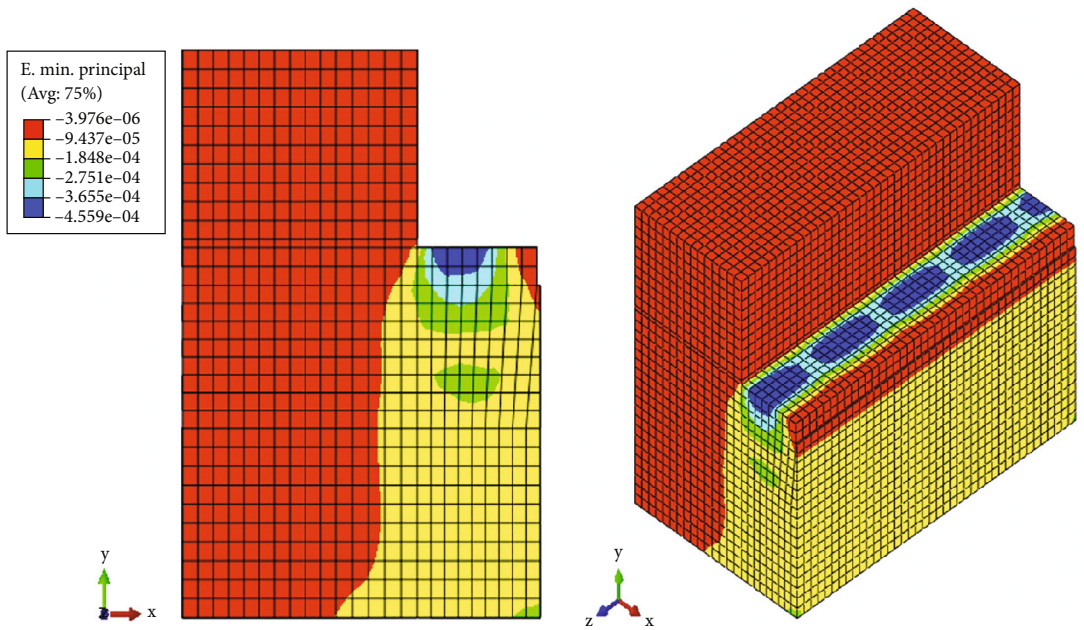

Figure 22: Compressive unit deformation of the model (the maximum compressive unit deformation/strain is 4.6×10^{-6}).

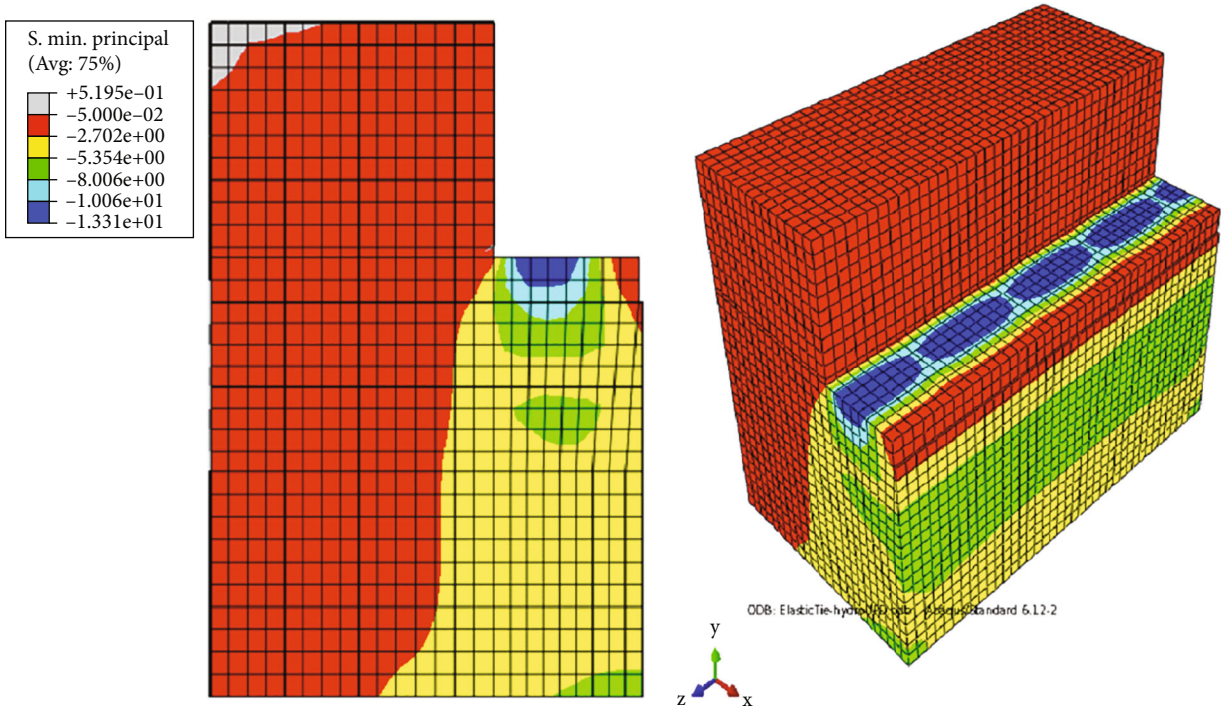

Figure 23: Maximum compressive stresses (maximum value 13.31 MPa, value in the first and second phases between 5 and 8 MPa).

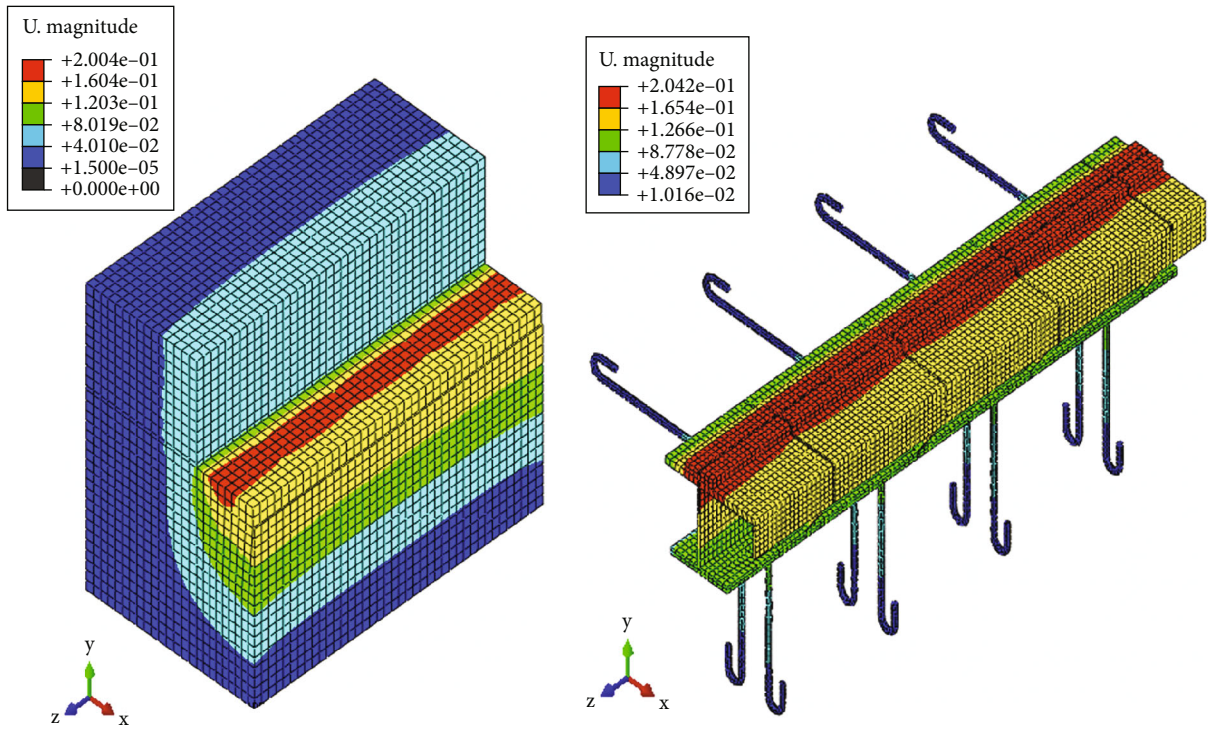

Figure 24: Maximum displacement due to the applied pressure (maximum displacement: 0.2 mm).

bond-slip behavior at the interface by inserting a cohesive interface element with a thickness of zero [18].

The dimensions of the concrete used for the modelling are shown in Figure 12. The dimensions of the steel sections, plates, and anchors are shown in Figure 13 for a 2 m long component. The 3D finite element modelling of the steel plates and anchors is shown in Figure 14.

The area under which the gate load is applied is the concrete mass. It is limited to a volume of 1165 mm ∗ 1500 mm ∗ 2000 mm. The part cut out for the finite element

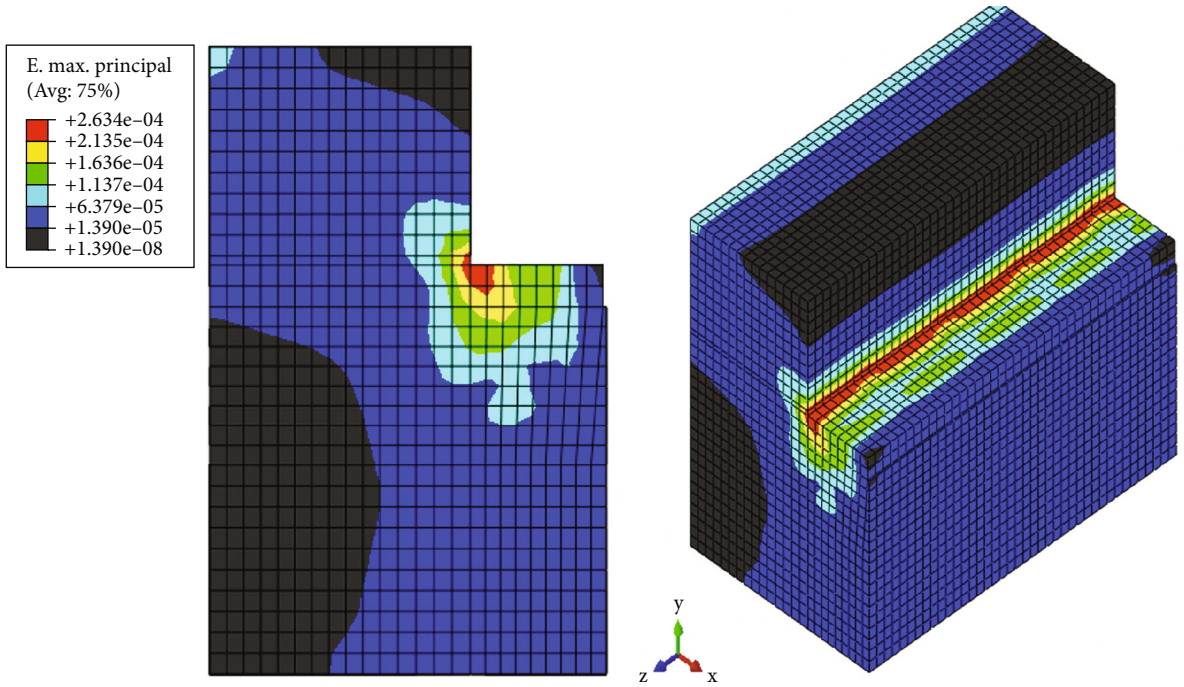

Figure 25: Tensile unit deformation/strain (maximum unit deformation: 2.63×10^{-4}).

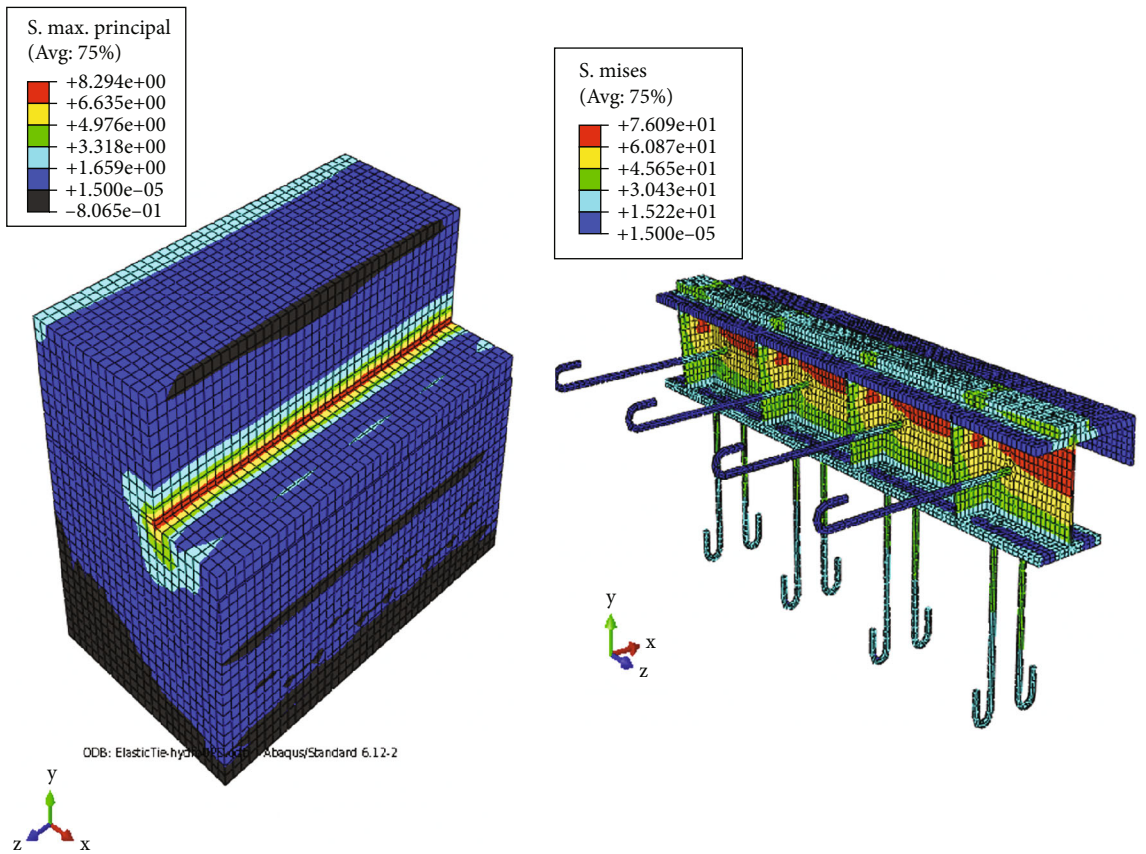

Figure 26: Tensile stresses under compression (maximum stress in concrete: between 6.63 and 8.29 MPa, maximum tensile strength in steel: 76 MPa).

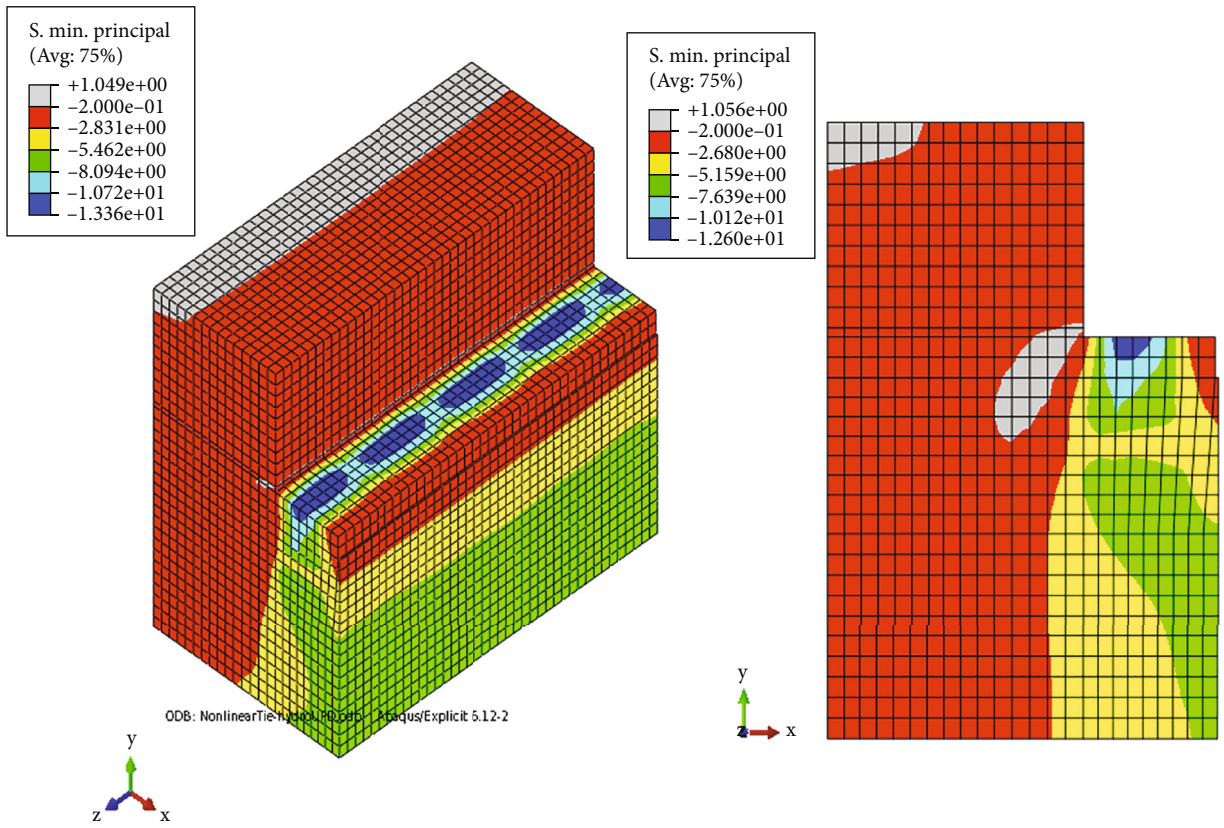

Figure 27: Concrete stresses in the nonlinear analysis (maximum compressive stress: 13.4 MPa).

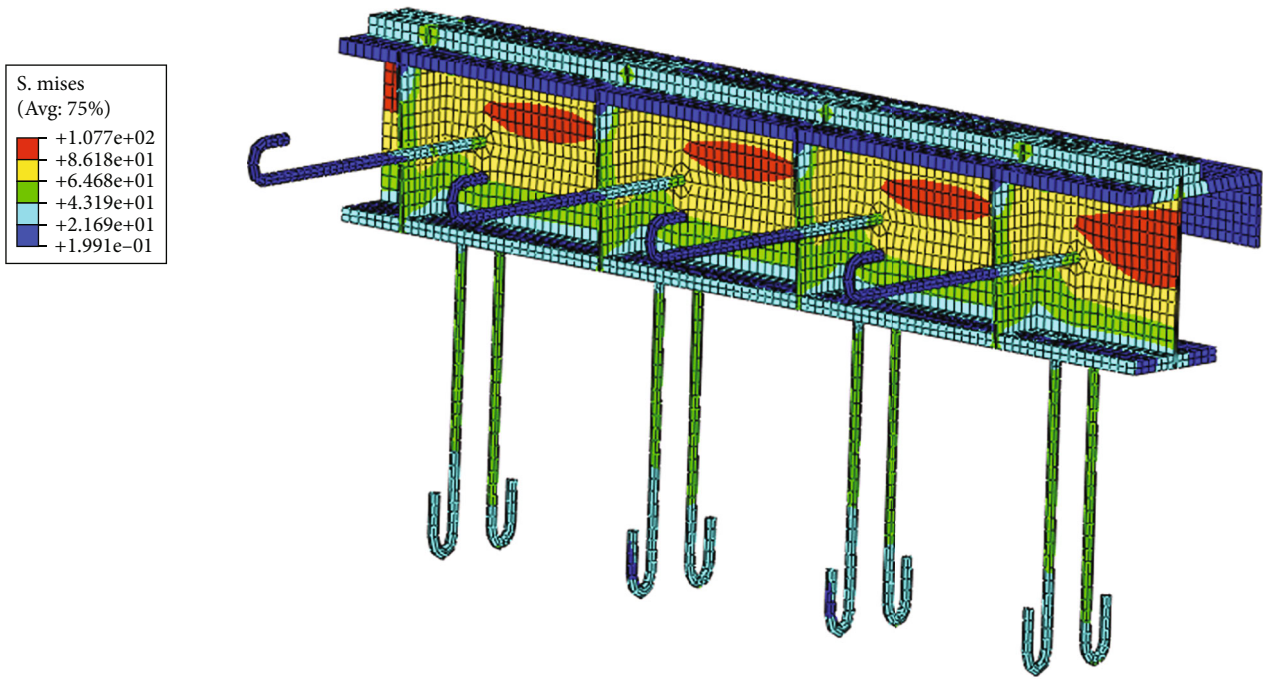

Figure 28: Stresses in steel in the nonlinear analysis (maximum stress: 108 MPa).

model was assumed to be a fixed bearing. The load and boundary conditions of the structure are shown in Figure 15, and the boundary conditions of the finite element model are shown in Figure 16.

The material models for the nonlinear analysis of the concrete and the elastoplastic behavior of steel are shown in Figures 17 and 18, respectively. The ultimate compressive strength of C25 is 25 MPa, and the tensile strength 1.75 MPa

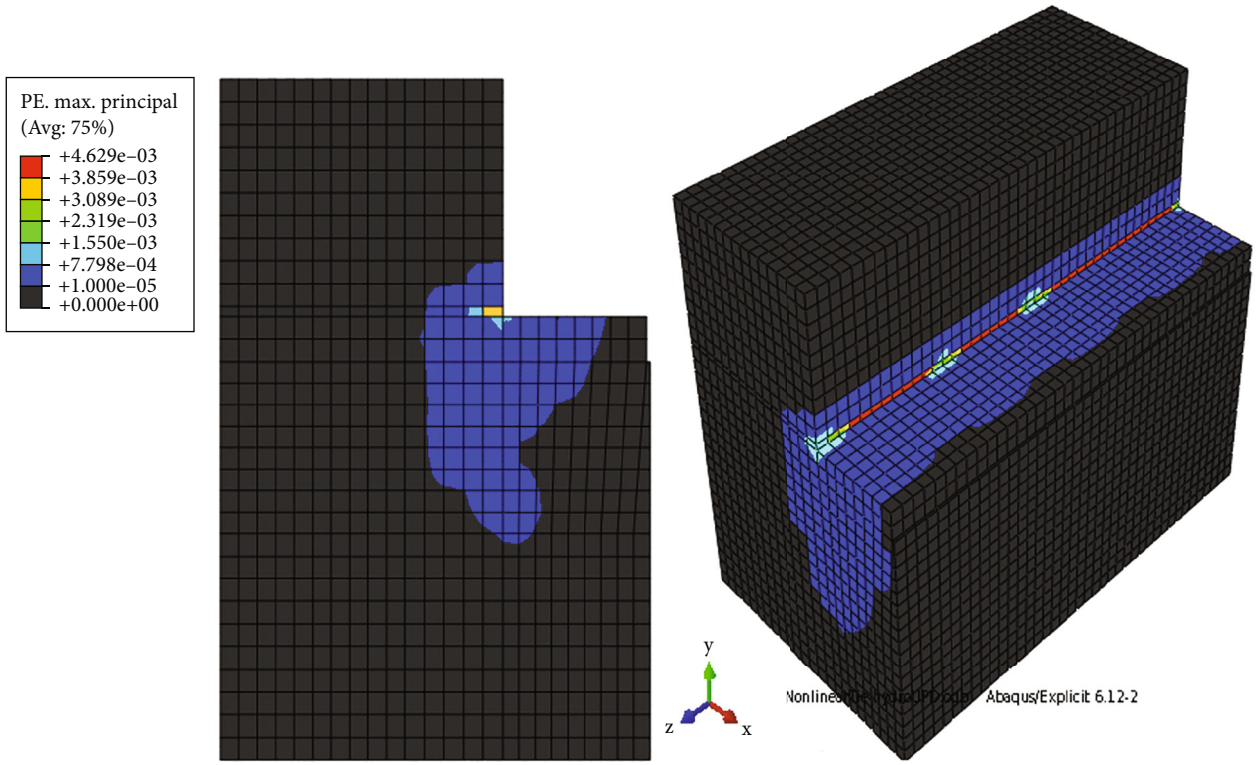

Figure 29: Deformations in the nonlinear analysis.

is used for the nonlinear analysis. The material properties of the concrete (C25), steel sections (St37), and reinforcement (StI) are used for linear and nonlinear analysis (see Table 1). The modulus of elasticity of the concrete C25 is used with 30000 MPa for the linear analysis and with 23500 MPa in the Popovich model for the nonlinear analysis. The modulus of elasticity of the steel sections (St37) is 206180 MPa and 200000 MPa for the anchor reinforcement. Poisson's ratio is assumed to be 0.2 and 0.3 for concrete and steel, respectively.

3.1. Applied Loads and Simple Stress Analysis for Simulation of the Gate Structure. The applied pressure loads as hydrostatic loads are shown in Figure 19. For a simple load and stress control of the gate at a maximum hydrostatic load at a water level of 85 meters, the maximum hydrostatic water pressure on the side surfaces and the concrete top layer, which comes after the plate, is shown in Figure 19 as $Q1$ and $Q2$:

$$Q1 = 85\,\text{m} \times 1000 \times 9.8 = 833\,\text{kPa}. \quad (1)$$

Load and pressure due to the plate on which each gate stands are as follows:

$$F = 85\,\text{m} \times 8\,\text{m} \times 10\,\text{kN/m}^3 = 3400\,\text{kN},$$
$$Q2 = \frac{F}{A} = \frac{3400\,\text{kN}}{1\,\text{m} \times 0.12\,\text{m}} = 28333\,\text{kPa}. \quad (2)$$

When calculating the pressure area of the gate, the pressure area on the upper side was calculated as $7.75 \times 0.125 = 0.96875\,\text{m}^2$. The total discharge area of the gate is $5.78125\,\text{m}^2$. $9.625 \times 0.5 = 4.8125\,\text{m}^2$ of this area must be the lateral pressure area. When calculating the area on which the load is transferred from the gates to the support, as shown in Figure 15, the load is not transferred from the gate to the upper support surface, as this section is only closed with a seal (Figure 20) and does not serve as a complete support. For this reason, this section was not included in the calculations (to be on the safe side).

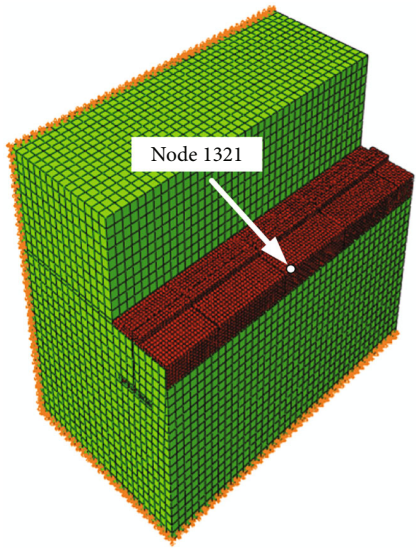

Figure 30: Location of reference node number 1321.

The points at which the gate exerts pressure on the side supports are shown in Figures 15 and 19. If both side

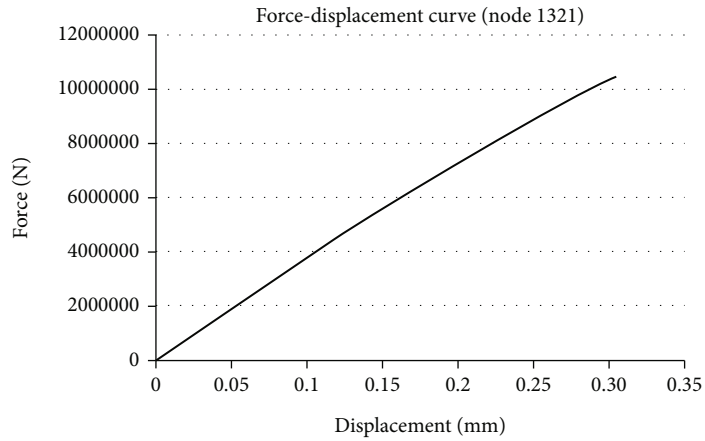

Figure 31: Force-displacement curve of node number 1321.

supports are considered, the total area to which the gate loads are transferred to the side supports is $9.625 \times 0.40 \times 2 = 7.70\,\text{m}^2$. Figure 21 shows that the load distribution is composed due to the I-shaped steel profile in the lateral supports that contains the bolts and anchors in the concrete.

The load is transferred from the gate to the supports: the compressive force on the supports is simply calculated as follows: $P = 85.00 \times 7.75 \times 10.00 = 6587.50$ tons (the height of the water is 85 meters). Taking into account the hydrostatic pressure on the concrete in the support area, the support area to which the load is transferred (considering the load on the gate) is as follows:

$$\sigma = \frac{P}{A} = \frac{6587.50}{7.70} = 855.52\,\text{t/m}^2. \quad (3)$$

The quality of the concrete was specified as C25 (25 MPa, 2500 t/m^2). According to TS500/2000 [19] Article 6.2.5, the coefficient of the concrete material in the case of the collapse analysis of the existing structure is assumed to be 1.0. If this coefficient is 1.0, the concrete compressive stress to be used for the calculation is 2500 t/m^2. The calculated concrete compressive stress (855.52 t/m^2) is less than 2500 t/m^2, so no concrete crush will occur.

The concrete compressive stresses determined above were calculated using simple methods and do not exceed the limit values. The real load distribution and the stresses are analyzed using the 3D finite element method and the ABAQUS program. The maximum concrete compressive stress determined in these analyses is below the value for the maximum compressive stress, and there is no crushing of the concrete as in the results of the nonlinear analysis of ABAQUS.

4. Linear and Nonlinear Simulations for Cracking and Collapse of Structure

4.1. Linear Analysis of the Gate Structure. The maximum and minimum pressures, tensile stresses, and unit deformations are shown in Figure 22. The maximum compressive deformation is 4.6×10^{-6}. The maximum permissible compressive deformation of this concrete is 3.5×10^{-3}. The unit deformation between the concrete of the first and second phases is between 1.8×10^{-4} and 9.4×10^{-5} (Figure 22). The maximum compressive stress is 13.31 MPa, and the compressive stress between the first and second phases is between 5 and 8 MPa (Figure 23). The maximum displacement due to the applied pressure is 0.2 mm, as you can see in Figure 24.

The maximum tensile deformation per unit is 2.63×10^{-4} (Figure 25). This shows that the concrete has exceeded the linear limit. Therefore, the nonlinear analysis was preferred for the capacity analysis. The maximum tensile stress in concrete is between 6.63 and 8.29 MPa. The maximum tensile stress in steel structures is 76 MPa. The tensile stress between the concrete of the first and second phases is between 1.5×10^{-5} and 1.66 MPa (see Figure 26).

4.2. Nonlinear Analysis of Gate Structure. The results of the nonlinear analysis are shown below. For the nonlinear analysis, the material properties given in Figure 17 for concrete and in Figure 18 for steel are used. The "Concrete Damage Model/Concrete Damage Plasticity Model" and the "Tension Stiffening" model in ABAQUS are considered.

In the nonlinear analysis, the maximum compressive stress of the concrete is given as 13.4 MPa (Figure 27). This value is lower than 25 MPa, the maximum strength of the concrete. The maximum stresses of the steel in the nonlinear analysis are 108 MPa (Figure 28). The deformations in the nonlinear analysis of the gate structure are shown in Figure 29.

4.3. Simulations for Nonlinear Capacity Analysis of Gate Structure. Simulations for the nonlinear analysis have shown that the system does not collapse at a water height of 85 meters. To see whether the system collapses or not, the loads were increased by 1.5 times and the following nonlinear capacity analysis of the gate structure was performed.

The system does not collapse even under 1.5 times the load. For the capacity analysis, the force-displacement curve of the reference node number 1321 (Figure 30) is examined in the model, as shown in Figure 31. The loads are gradually increased, considering the force-displacement curve for nonlinear behavior. This analysis shows that the system continues to support the load and does not collapse. According to this curve, the system has not

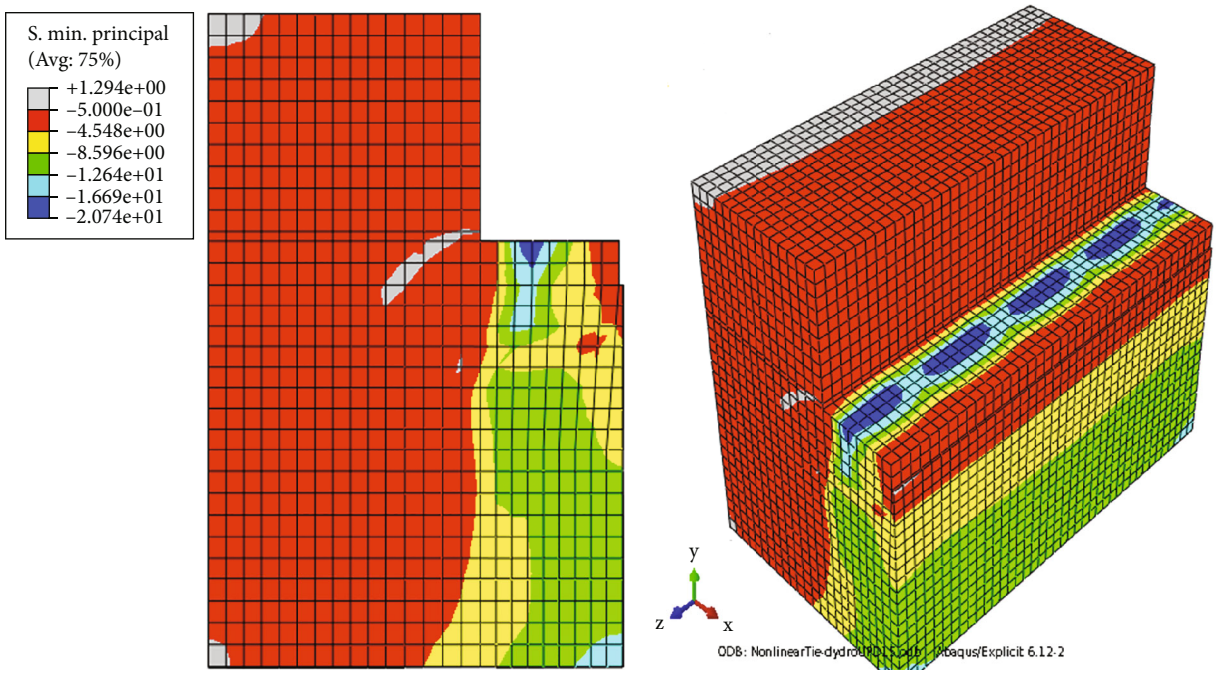

Figure 32: Compressive stress distribution at 1.5 times load (maximum stress: 20 MPa).

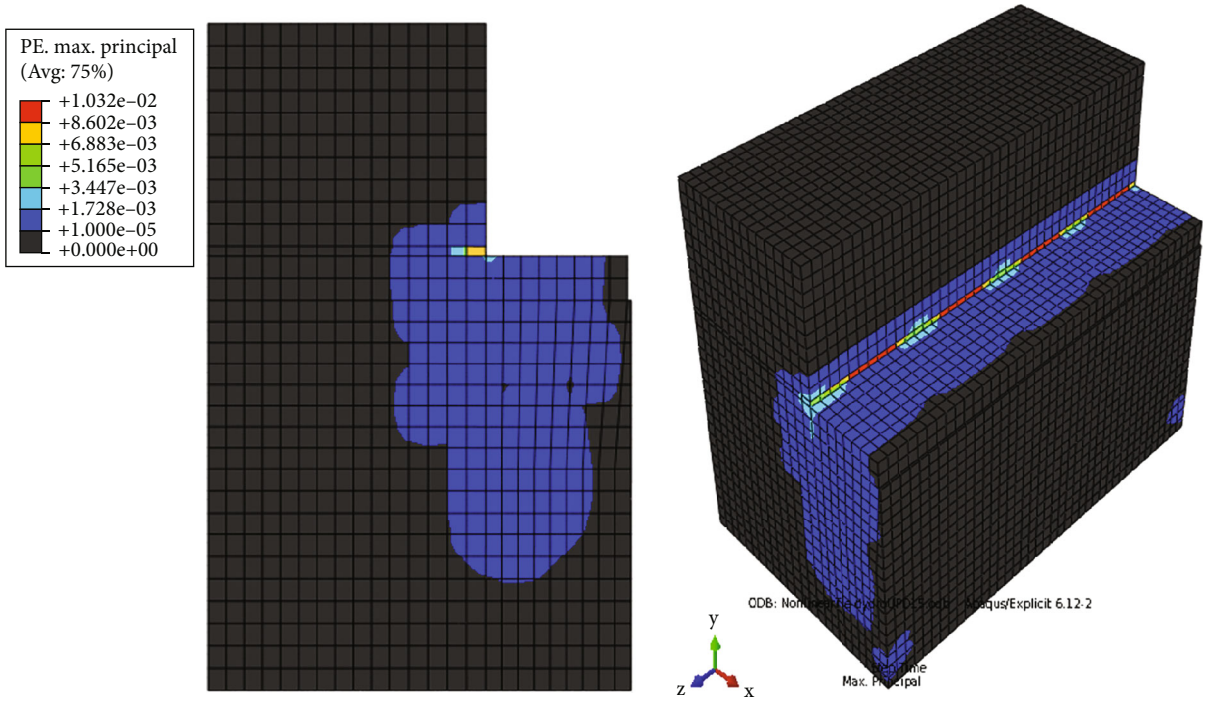

Figure 33: Deformations at 1.5 times loads for the capacity check.

collapsed when it is under load and has reached its maximum value. The maximum compressive stress of the concrete is 20 MPa, and the stress distribution is shown in Figure 32 when the hydrostatic load at 85 m is increased by one and a half times. This compressive stress is lower than the maximum strength of the concrete C20/25. On the other hand, it was found that the deformation limits of the concrete were exceeded in some local areas, as can be seen in Figure 33.

5. Conclusions

In this study, a nonlinear analysis method is used to simulate the real behavior of the structure under hydrostatic loading.

The nonlinear 3D modelling uses C3D8R elements with reduced integration and 8 hexahedral nodes and considers the concrete damage model/concrete damage plasticity model and the tension stiffening model in ABAQUS. The analysis of the limit state collapse should be performed using a nonlinear finite element analysis method that takes into account the real behavior of a composite system and the principle of stress redistribution.

A nonlinear capacity analysis of the gate structure was carried out. The loads were gradually increased up to 1.5 times the hydrostatic forces, and the force-displacement curve was plotted for a reference point in the finite element model. It turned out that the concrete compressive stresses of 20 MPa determined in the calculations were lower than the maximum compressive stress of the concrete, namely, 25 MPa, and that no collapse or crushing of the concrete occurred. On the other hand, the nonlinear capacity analyses and investigations showed that the deformation limits of the concrete were exceeded in some local areas.

In the nonlinear 3D finite element analysis, the anchorages between the concrete of the first and second phases of the gate structure and the steel profiles in the support areas where the gates were subjected to hydrostatic loads are also included according to the project details, considering the construction phases, to obtain the actual load and stress distribution. The results of the analysis showed that the bond behavior of the system with the bonding and the nonlinear behavior of the concrete influenced the results. It was found that these steel anchors carry very large loads and allow the composite system to act with a bond. Therefore, the nonlinear 3D finite element modelling, analysis, and design of the composite system with the modelling of the anchors and steel sections are important for the load transfer of tunnel diversion structures and gates.

Diversion tunnel gates of a dam are the critical part of a dam's safety structures. It is suggested that dam monitoring and control systems can be used to assess and control the gates of a dam according to the water level and water flow rate, monitor the erosion in the tunnel, and control the problems with the advantages of artificial intelligence applications and warning systems. The use of multiple gates is also recommended if a problem occurs in the operation of a gate in the diversion tunnels of a dam to ensure the safety of the tunnel gates in dam structures.

For future studies, the developed model can also be validated by experimental tests with prototypes. The validation of the model is done by checking simple load and stress and strain hand calculations in engineering considering the structural behavior of the tunnel gates observed in the finite element modelling and simulations in this work. The quality of the concrete in the diversion of the tunnel gate of the dam structure was determined based on the core test results of in situ concrete specimens.

Data Availability

All data, models and codes generated or used are included in the article.

Conflicts of Interest

The author declares that there are no conflicts of interest.

References

[1] P. C. F. Erbisti, *Design of Hydraulic Gates*, CRC Press, Taylor and Francis Group, London, UK, 2nd edition, 2014.

[2] K. Sahu and S. Ajmera, "Design of radial gate using rectangular and I-sections- a case study," *International Journal of Advances in Scientific Research and Engineering (IJASRE)*, vol. 3, no. 2, pp. 1–10, 2017.

[3] Ç. I. Unal, *Two-Dimensional Dam Break Analysis of Berdan Dam*, M. Sc. in the Department of Civil Engineering, Middle East Tech University (METU), 2019.

[4] R. S. Kharche, G. P. Ptil, and N. A. Kharche, "Design and analysis of lifting mechanism of dam gate opening hoist machine," *International Research Journal of Engineering and Technology (IRJET)*, vol. 2, no. 8, pp. 130–135, 2015.

[5] DSI Dam Construction Technical Code (in Turkish), *General Directorate of State Water Works_R00_20061110*, State Hydraulic Works, Turkey, 2006.

[6] Bureau of Reclamation, "Valves, gates and steel conduits," *Design Standards*, vol. 7, 1956.

[7] "Design standards no.6 hydraulic and mechanical equipment," in *Chapter 6: Bulkhead Gates and Stoplogs Phase 4*, US Department of the Interior Bureau of Reclamation, 2018.

[8] M. G. Hailu and A. Thakur, "Design analysis of water control gate for diversion dams," *International Journal of Current Engineering and Technology*, vol. 8, no. 3, pp. 708–718, 2018.

[9] E. A. Hammack, R. L. Stockstill, and J. Vaughan, "Design concept and analysis for a navigation gate guard," in *US Army Engineering Research and Development Center (ERDC)*, pp. 1–12, Coastal and Hydraulics Lab. Vicksburg, MS, Report ERDC/CHL CHETN-IX-25, 2011.

[10] S. Ma, Y.-q. Chen, Z.-q. Wang, S.-t. Li, Q. Zhu, and L.-m. Chen, "The damage to model concrete gravity dams subjected to water explosions," *Defence Technology*, vol. 27, pp. 119–137, 2023.

[11] A. J. Moradloo, A. Adib, and A. Pirooznia, "Damage analysis of arch concrete dams subjected to underwater explosion," *Applied Mathematical Modelling*, vol. 75, pp. 709–734, 2019.

[12] J. Lee and G. L. Fenves, "A plastic-damage concrete model for earthquake analysis of dams," *Earthquake Engineering & Structural Dynamics*, vol. 27, no. 9, pp. 937–956, 1998.

[13] Y. Huang, Z. Yang, W. Ren, G. Liu, and C. Zhang, "3D meso-scale fracture modelling and validation of concrete based on in-situ X-ray computed tomography images using damage plasticity model," *International Journal of Solids and Structures*, vol. 67, pp. 340–352, 2015.

[14] Y. J. Huang, Z. J. Yang, X. W. Chen, and G. H. Liu, "Monte Carlo simulations of meso-scale dynamic compressive behavior of concrete based on X-ray computed tomography images," *International Journal of Impact Engineering*, vol. 97, pp. 102–115, 2016.

[15] ABAQUS/CAE User's Manual, *Version 6.12, Hibbitt Karlsson & Sorensen*, Simulia Inc., USA, 2011.

[16] ABAQUS, *6.12 Keywords Reference Manual*Dassault systems, Simulia Corp, Province, RI, USA.

[17] L. Hai, Y.-J. Huang, P. Wriggers, H. Zhang, and Q.-H. Li, "Investigation on fracture behaviour of UHPFRC using a mesoscale computational framework," *Computer Methods in Applied Mechanics and Engineering*, vol. 421, article 116796, 2024.

[18] H. Zhang, Y.-j. Huang, S.-l. Xu, S. Natarajan, and F. Yao, "An explicit methodology of random fibre modelling for FRC fracture using non-conforming meshes and cohesive interface elements," *Composite Structures*, vol. 310, article 116762, 2023.

[19] *TS500 Requirements for Design and Construction of Reinforced Concrete Structures*, TSE, Turkish Standard, 2000.